doi:10.1038/nature04474

LETTERS

NMDA receptors mediate calcium accumulation in myelin during chemical ischaemia

I. Micu[1], Q. Jiang[1], E. Coderre[1], A. Ridsdale[1], L. Zhang[1], J. Woulfe[1], X. Yin[2], B. D. Trapp[2], J. E. McRory[3], R. Rehak[3], G. W. Zamponi[3], W. Wang[1] & P. K. Stys[1]

Central nervous system myelin is a specialized structure produced by oligodendrocytes that ensheaths axons, allowing rapid and efficient saltatory conduction of action potentials[1]. Many disorders promote damage to and eventual loss of the myelin sheath, which often results in significant neurological morbidity. However, little is known about the fundamental mechanisms that initiate myelin damage, with the assumption being that its fate follows that of the parent oligodendrocyte. Here we show that NMDA (*N*-methyl-D-aspartate) glutamate receptors mediate Ca^{2+} accumulation in central myelin in response to chemical ischaemia *in vitro*. Using two-photon microscopy, we imaged fluorescence of the Ca^{2+} indicator X-rhod-1 loaded into oligodendrocytes and the cytoplasmic compartment of the myelin sheath in adult rat optic nerves. The AMPA (α-amino-3-hydroxy-5-methyl-4-isoxazole propionic acid)/kainate receptor antagonist NBQX[2] completely blocked the ischaemic Ca^{2+} increase in oligodendroglial cell bodies, but only modestly reduced the Ca^{2+} increase in myelin. In contrast, the Ca^{2+} increase in myelin was abolished by broad-spectrum NMDA receptor antagonists (MK-801, 7-chlorokynurenic acid, D-AP5[3,4]), but not by more selective blockers of NR2A and NR2B subunit-containing receptors (NVP-AAM077[5] and ifenprodil[2,4]). *In vitro* ischaemia causes ultrastructural damage to both axon cylinders and myelin[6]. NMDA receptor antagonism greatly reduced the damage to myelin. NR1, NR2 and NR3 subunits were detected in myelin by immunohistochemistry and immunoprecipitation, indicating that all necessary subunits are present for the formation of functional NMDA receptors. Our data show that the mature myelin sheath can respond independently to injurious stimuli. Given that axons are known to release glutamate[7–9], our finding that the Ca^{2+} increase was mediated in large part by activation of myelinic NMDA receptors suggests a new mechanism of axo–myelinic signalling. Such a mechanism may represent a potentially important therapeutic target in disorders in which demyelination is a prominent feature, such as multiple sclerosis, neurotrauma, infections (for example, HIV encephalomyelopathy) and aspects of ischaemic brain injury.

We measured $[Ca^{2+}]$ changes from the cytosolic compartment of compact myelin (the space of compact myelin between the cytoplasmic leaflets of the spiralled myelin membranes, the 'major dense line') and oligodendroglial cell bodies in live adult rat optic nerves (Fig. 1). Nerves were rendered chemically ischaemic by using the mitochondrial inhibitor NaN_3 and omitting glucose. Ca^{2+}-dependent fluorescence from myelin regions ($F_{Ca.my}$) began to increase within minutes of the onset of ischaemia and rose to 50 ± 22% above baseline after 30 min (mean ± s.d., $n = 94$ myelin regions from individual axons). Ca^{2+}-dependent fluorescence from oligodendroglial cytoplasm ($F_{Ca.ol}$) rose with a similar time course, increasing by 43 ± 27% ($n = 53$) above control at 30 min. Removal of bath Ca^{2+} abolished both the myelinic and oligodendroglial ischaemic Ca^{2+} increase (Fig. 1f), indicating that in both compartments, Ca^{2+} increases are mainly a result of influx from the extracellular space.

We then explored potential routes of Ca^{2+} entry into both oligodendrocytes and myelin. Kynurenic acid (1 mM), a broad-spectrum antagonist of ionotropic glutamate receptors, completely blocked the increase in $F_{Ca.ol}$ (−8 ± 8% of baseline at 30 min ischaemia, $n = 10$, $P = 1.6 \times 10^{-6}$ versus drug-free ischaemia) and $F_{Ca.my}$ (−1 ± 16%, $n = 29$, $P = 2.0 \times 10^{-6}$). The more selective AMPA/kainate receptor antagonist NBQX (30 μM) completely blocked the rise in $F_{Ca.ol}$ (−5 ± 11% of control at 30 min, $n = 33$, $P = 1.6 \times 10^{-6}$) but had only a modest effect on myelinic Ca^{2+} rise (40 ± 18%, $n = 57$ in NBQX versus 50 ± 22% in drug-free ischaemia, $P = 0.003$; Fig. 2). This finding has two important implications. First, the fact that an AMPA/kainate receptor antagonist is able to dissociate the ischaemic Ca^{2+} increase in the two compartments indicates that the myelinic Ca^{2+} increase is not merely a passive phenomenon attributable to diffusion of Ca^{2+} from the parent cell body, but is instead mediated by a distinct mechanism. Second, the pharmacological profile suggests an unexpected route of Ca^{2+} influx into myelin. Although AMPA and kainate receptors are known to be present and functional in white matter glia, NMDA receptors are generally thought to be absent[10]; yet the above results suggest that NMDA receptors mediate ischaemic Ca^{2+} rise in the myelin sheath.

To explore this possibility more directly, we treated ischaemic optic nerves with selective NMDA receptor antagonists. The non-competitive channel blocker MK-801 (10 μM), and competitive glutamate (D-AP5, 100 μM) and glycine (7-chlorokynurenic acid, 200–500 μM) site antagonists[3], completely blocked the increase in myelinic Ca^{2+}(−1 ± 19%, $n = 50$ for MK-801; −16 ± 17%, $n = 103$ for D-AP5; −20 ± 14%, $n = 45$ for 7-chlorokynurenic acid at 30 min, versus 50 ± 22% without drug; $P = 2.1 \times 10^{-6}$ for all groups; Fig. 2c). All three agents also reduced the ischaemic Ca^{2+} increase in oligodendrocyte cell bodies (20 ± 35%, $n = 20$, $P = 0.0002$; −20 ± 20%, $n = 49$, $P = 1.8 \times 10^{-6}$; −22 ± 23%, $n = 23$, $P = 1.8 \times 10^{-6}$, respectively, versus 43 ± 27% without drug), suggesting that NMDA receptors may also directly admit Ca^{2+} into these cells. This is consistent with the observation of NMDA-induced currents in rat spinal cord oligodendrocytes[11].

Functional NMDA receptors are heteromers composed of NR1 and NR2 subunits, which express the glycine and glutamate recognition sites, respectively[2,4]. Discovered more recently, the NR3 subunit may serve a modulatory role[12]. A number of splice variants have been identified for each subunit, resulting in a potentially very diverse family of receptors. More specific blockers of NR2A- and

[1]Ottawa Health Research Institute, Division of Neuroscience and Department of Cellular and Molecular Medicine, University of Ottawa, Ottawa, Ontario K1Y 4K9, Canada. [2]Department of Neurosciences, Cleveland Clinic Foundation, Cleveland, Ohio 44195, USA. [3]Department of Physiology and Biophysics, Hotchkiss Brain Institute, University of Calgary, Alberta T2N 4N1, Canada.

NR2B-containing receptors (NVP-AAM077[5], tested at 0.4–5 μM; ifenprodil[4], 10 μM) did not significantly reduce the ischaemic increase in $F_{Ca.my}$ (43 ± 14%, $n = 22$ for 0.4 μM NVP; 63 ± 34%, $n = 28$ for ifenprodil, versus 50 ± 22% without antagonist) (Fig. 2c). Taken together, our pharmacological data suggest that NMDA receptors (possibly those not composed of NR2A or NR2B subunits) mediate the bulk of pathological Ca^{2+} accumulation into the myelin sheath of adult optic axons. This is in contrast to oligodendrocytes, in which Ca^{2+} increase and cell death are mediated mainly, but possibly not exclusively (see above), by glutamate receptors of the AMPA/kainate class as previously reported[13] (but see ref. 14).

We next used immunohistochemistry to localize NMDA receptor subunits (Fig. 3). NR1 subunits were detected just outside axon cylinders. Because virtually all adult rat optic axons are myelinated, regions immediately adjacent to axon cylinders represent myelin. NR2 and NR3 showed a similar distribution. Staining for all three subunits often appeared in discrete high densities in myelin of larger axons. Immunoelectron microscopy detected labelling of myelin internodes with antibodies against NR1, NR2 and NR3 (Fig. 3e–g), with gold particles conspicuous in the inner and outer margins of myelin. Furthermore, NR1 was detected on the rough endoplasmic reticulum and Golgi membranes located in the perinuclear cytoplasm of oligodendrocytes (Fig. 3h), supporting the idea of NR1 synthesis by the myelin-forming cell.

We extracted the myelin fraction from whole optic nerve on a sucrose gradient (see Supplementary Methods). NR1, NR2 and NR3

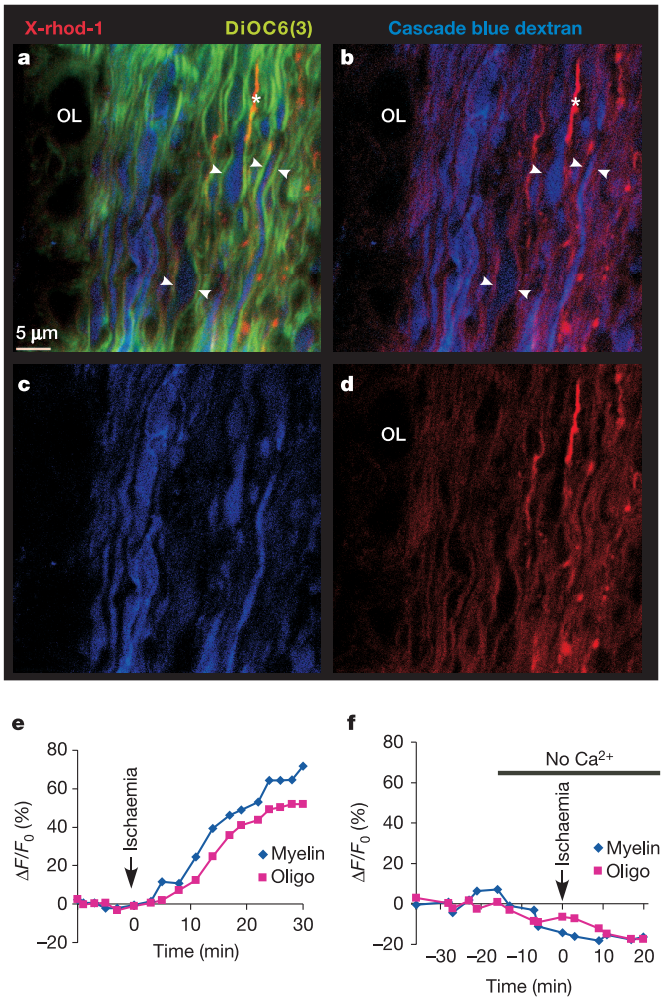

Figure 1 | Ca^{2+} imaging in optic nerve oligodendrocytes and myelin. **a**–**d**, The same image is shown, but with various colour channels suppressed. Cascade blue dextran outlines axon cylinders, DiOC6(3) strongly stains myelin (arrowheads in **a**), and X-rhod-1 partitions into myelin (arrowheads in **b**) and oligodendrocytes (OL). Glial processes unstained by DiOC6(3) (asterisk in **a** and **b**) were excluded. **e**, Representative time course of X-rhod-1 fluorescence change in oligodendrocytes and myelin. Fluorescence began to increase in both compartments within minutes of ischaemia, rising to ~50–60% above control levels after about 30 min. **f**, This increase was prevented in Ca^{2+}-free aCSF (with 1 mM EGTA added to chelate residual Ca^{2+}), indicating that Ca^{2+} increase in oligodendrocytes and myelin depends on influx from the extracellular space.

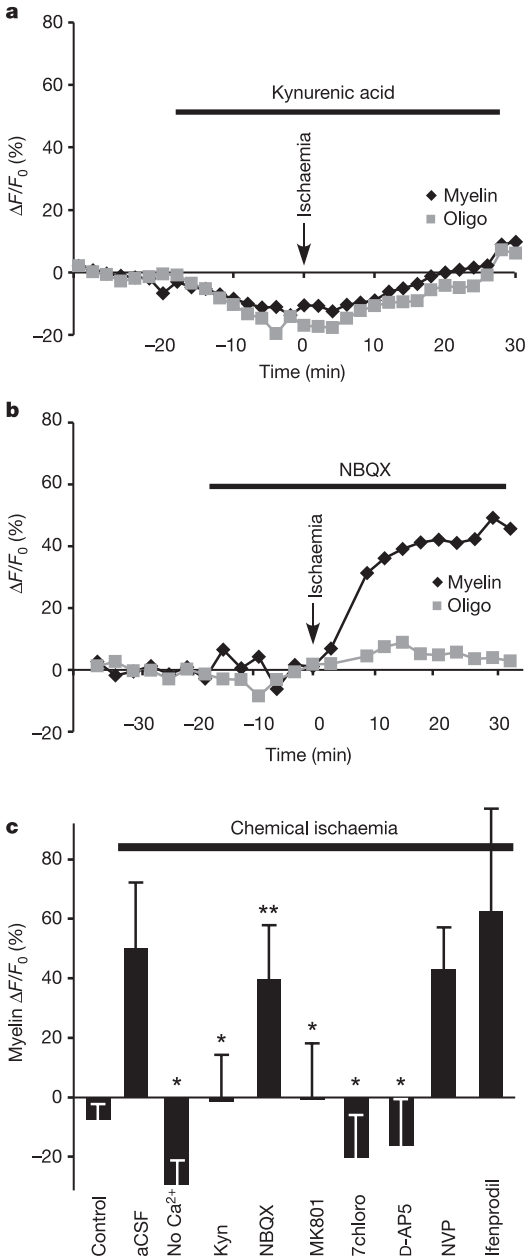

Figure 2 | Effects of glutamate receptor antagonists on ischaemic Ca^{2+} increase. **a**, Kynurenic acid greatly reduced the ischaemic Ca^{2+} increase in both oligodendrocytes and myelin (compare to Fig. 1e). **b**, NBQX blocked the Ca^{2+} increase in oligodendrocytes much more potently than in myelin. **c**, Bar graph summarizing X-rhod-1 fluorescence change (mean ± s.d.) at 30 min of ischaemia compared to pre-ischaemic/pre-drug baseline. Together, these data indicate that NMDA receptors are largely responsible for myelinic Ca^{2+} accumulation. $^{*}P < 10^{-5}$; $^{**}P = 0.003$ versus drug-free ischaemia (aCSF) (±DMSO as applicable). For each treatment group, 29–104 myelin regions of interest from at least three different experiments were analysed.

subunits could not be detected in the unpurified fraction (not shown). After immunoprecipitation, however, we were able to detect NR1-, NR2- and NR3-positive bands at the expected molecular masses by immunoblotting. Moreover, NR2 and NR3 subunits were detected in lysate precipitated by NR1 antibodies from the myelin fraction (Fig. 3i). We note that the NR2 blot revealed a band of approximately 140 kDa, which, given the known cross-reactivity of the antibody used (see Supplementary Methods), could be consistent with NR2C and/or NR2D subunits. Overall, our biochemical analysis supports the hypothesis that myelin expresses functional NMDA receptor complexes.

The expression of functional NMDA receptors in the mature myelin sheath and their ability to mediate ischaemic Ca^{2+} accumulation suggests that these receptors may have an important role in the degeneration of myelin, and may be an early trigger for eventual demyelination. Examination of ischaemic optic nerve axons by electron microscopy showed marked destruction of axoplasmic constituents, with disappearance of microtubules and neurofilament profiles[6] (Fig. 4). In addition, the myelin sheath began to split focally (Fig. 4a, arrowheads), with loosening and separation of the lamellae. NMDA receptor inhibition significantly reduced the pathological changes in the myelin sheath; in contrast, there was little evidence that axon cylinders *per se* were protected, indicating that these elements are damaged by another mechanism (Fig. 4b). This finding is consistent with our observation that NMDA receptor block failed to blunt axoplasmic (as opposed to myelinic) Ca^{2+} increase during ischaemia (Supplementary Fig. 3).

Myelin is a vital structure that has been observed histopathologically to degenerate in a broad range of CNS disorders[15]. These demyelinated central axons conduct aberrantly or not at all, and account for significant clinical morbidity. During development, reciprocal axo–glial signalling has a key role in the initiation and completion of myelination[16]. In contrast, little is known about the signalling that may take place between axons and the mature myelin sheath. Numerous studies have demonstrated the presence of many enzymes[17] (including Na^+,K^+-ATPase[18]), connexins[19] and AMPA/kainate receptors[20,21] in mature myelin, suggesting that this structure may be more dynamic and metabolically active than previously thought, actively participating in signal transduction and translocation of ions and small molecules. Here we show that mature myelin is compromised by ischaemia and that Ca^{2+} ions accumulate in its cytosolic domain in an NMDA receptor-dependent fashion. Given the presence of Ca^{2+}-sensitive enzymes such as calpain-1 and phospholipase C in central myelin[17,22], it is possible that such Ca^{2+} accumulation then promotes degradation of a number of key structural myelin components.

NMDA receptors must bind both glutamate and glycine as obligatory co-agonists, and activation additionally requires depolarization to remove Mg^{2+}-dependent block[2,23]. Both neurotransmitters are taken back up into cells by electrogenic, Na^+-coupled transporters, which can operate in the reverse, transmitter efflux mode under conditions of increased intracellular [Na^+] and membrane depolarization[24,25]. Injured axons accumulate Na^+, lose K^+ and depolarize (see ref. 26 for a review), thus promoting the release of glutamate via this mechanism[8]. CNS myelinated axons have been shown to express glycine transporters as well[27]; therefore they could release this amino acid under pathological conditions in a manner analogous to glutamate. Together with ischaemic depolarization of cellular membranes, this would complete the requirements for sustained and deleterious activation of myelinic NMDA receptors.

NMDA receptors have fundamental roles in the normal physiology of the CNS[28] and in many diseases[4,29]. These receptors have not been

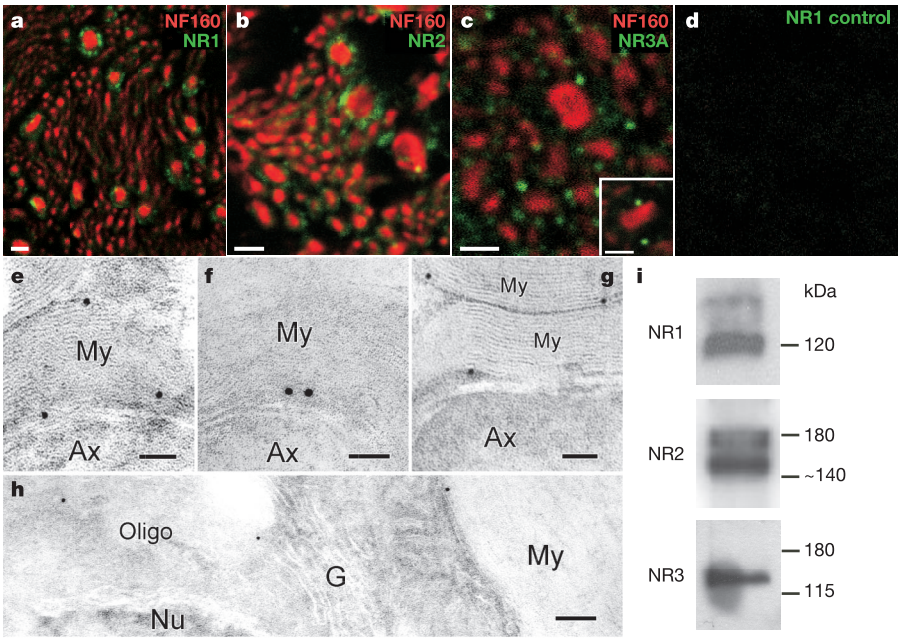

Figure 3 | Immunodetection of NMDA receptor subunits in myelin. **a**, Nerves were immunostained for neurofilament (NF)160 and NR1 subunits, and imaged by confocal microscopy. Most axons in adult nerves are myelinated, and therefore regions immediately outside axon cylinders represent myelin sheaths. Faint, homogeneous NR1 signal was seen just outside NF160-positive axon cylinders, and was most apparent in larger axons. Myelin of larger-diameter axons showed occasional punctate regions of more intense NR1 label. **b**, **c**, NR2 and NR3 subunits showed a similar distribution. Inset in **c** shows an example of punctate NR3A staining at the inner and outer myelin rim of a larger axon. **d**, Control with primary antibodies omitted. Controls for NR2 and NR3 were similar. **e**–**g**, Immunogold staining of optic nerve for NR1 (**e**), NR2 (**f**) and NR3 (**g**) showed specific myelin labelling (My), with enrichment of gold particles at the inner and outer margins of the sheath (Ax, axon). **h**, NR1 was also detected on the rough endoplasmic reticulum and Golgi membranes (G) in oligodendrocyte perinuclear cytoplasm (Nu, nucleus). **i**, A pan-NR1 monoclonal was used to immunoprecipitate receptor complexes from myelin fractions in all three blots, which were then probed with anti-NR1, anti-NR2 or anti-NR3 antisera. All three subunits were detected, and both NR2 and NR3 are complexed with NR1. Scale bars, 2 μm (**a**–**c**), 50 nm (**e**–**g**), 100 nm (**h**).

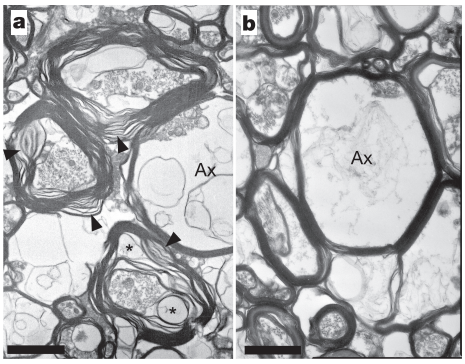

Figure 4 | NMDA receptor inhibition protects myelin against ischaemic injury. a, Vehicle-treated nerves showed marked damage to myelin after 60 min of *in vitro* chemical ischaemia, with separation of the compact lamellae (arrowheads), swellings and vacuolations (asterisks). Axon cylinders (Ax) were also severely damaged and swollen, with the disappearance of neurofilament and microtubule profiles. **b**, The NMDA receptor antagonist 7-chlorokynurenic acid (500 μM) protected myelin. Occasional focal loosening of the compact sheath was observed, but was much less pronounced compared to controls (2.0 ± 1.0 lamellar separations per 65 μm^2 in 7-chlorokynurenic acid versus 4.0 ± 1.4 in vehicle alone, $P = 0.0016$). In contrast, damage to axon cylinders (Ax) remained severe. Scale bars, 1 μm.

considered important in the physiology or pathobiology of white matter, but it is likely that their presence in myelin suggests a normal physiological role. Action potential traffic releases glutamate from axons[7,9], and glycine could also be released in an activity-dependent manner. If myelinic NMDA receptors are composed of NR2C and/or NR2D subunits, as our data suggest, they would be more sensitive to glutamate and glycine[2,4]. This would assist signalling in a system (myelinated axons) that is, in contrast to synapses, presumably less able to release large local amounts of transmitter. The activity-dependent release of axonal glutamate, in quantities reflecting an integral of ongoing electrical traffic in the sourcing fibre, might activate myelinic NMDA receptors to support axo–glial communication. This would represent an elegant solution for allowing axons, which may be conducting different volumes of impulse traffic, to selectively signal their myelin sheaths about their levels of activity. Such a signal could in turn be transduced to the parent oligodendrocyte for purposes of myelin production commensurate with the degree of electrical activity of individual fibres. Under pathophysiological conditions, excessive stimulation of myelinic NMDA receptors may cause direct Ca^{2+}-dependent damage to this structure. For instance, the NMDA receptor antagonist memantine[29] was reported to reduce neurological disability in a rat model of experimental autoimmune encephalomyelitis[30]. Although the mechanisms are not clear, it is possible that this agent reduced myelin damage by antagonizing the effects of glutamate released in the inflammatory lesions. A more in-depth understanding of such an NMDA-receptor-dependent 'axo–myelinic' communication could guide the design of more effective treatments for disorders in which demyelination of central white matter tracts is a prominent and clinically devastating phenomenon.

METHODS

Please refer to Supplementary Information for additional details.

Ca^{2+} imaging. Rat optic nerves from adult Long Evans rats were loaded with the Ca^{2+} indicator X-rhod-1 AM to report the free [Ca^{2+}] in myelin and oligodendrocytes, and with DiOC6(3) to outline myelin. Dextran-conjugated Ca^{2+}-insensitive cascade blue was selectively loaded into axons. Two-photon excited fluorescence images were collected every 2 min using a custom-modified Nikon D-Eclipse C1 laser scanning microscope. Emitted fluorescence was collected using appropriate filters. Image data were imported into ImageTrak software (written by P.K.S.; http://www.ohri.ca/stys/imagetrak) for analysis. All quantitative fluorescence changes are reported after a standard 30-min exposure to ischaemia. In-place immunohistochemistry of live nerves was performed to ascertain the localization of X-rhod-1. Fluorescence-lifetime measurements confirmed that fluorescence intensity of X-rhod-1 reported [Ca^{2+}] changes, and Mn^{2+} quench studies showed that emission originated from the cytosolic compartment of myelin (see Supplementary Methods).

Immunohistochemistry and immunoelectron microscopy. For light microscopy, deeply anaesthetized adult rats were perfused with saline then 4% paraformaldehyde in 0.1 M phosphate buffer. Optic nerves were post-fixed, placed in 20% sucrose overnight, then sectioned at a thickness of 30 μm in a cryostat. All washes were done in TBS/1% Triton X-100, and sections were blocked with 10% normal donkey serum, 3% dry milk for 1 h at 20 °C. Samples were incubated overnight in primary antibodies, then secondary antibodies were applied. Sections were imaged on a Nikon D-Eclipse C1 confocal microscope. Immunoelectron microscopy was performed using standard techniques as described in Supplementary Methods.

Immunoblots and immunoprecipitation. Myelin fractions were incubated on ice for 1 h, centrifuged for 15 min (4 °C) at 15,000 *g*, and the supernatant was collected for overnight dialysis against the binding solution (300 mM NaCl, 50 mM Tris pH 7.5 and 0.1% Triton X-100). Total protein (250 μg in 50 μl) was immunoprecipitated with a pan-NR1 monoclonal antibody. The complex was centrifuged, resuspended and loaded onto a 6% acrylamide SDS–PAGE gel. Samples were transferred to a PVDF membrane and western blot analysis was performed using a different NR1 polyclonal antibody, or NR2 or NR3 antisera. Appropriate negative controls were performed by omitting the primary (precipitating) antibody or probing with secondary antibody only (data not shown).

Received 20 August; accepted 29 November 2005.
Published online 21 December 2005.

1. Waxman, S. G., Kocsis, J. D. & Stys, P. K. *The Axon: Structure, Function and Pathophysiology* (Oxford Univ. Press, Oxford, 1995).
2. Dingledine, R., Borges, K., Bowie, D. & Traynelis, S. F. The glutamate receptor ion channels. *Pharmacol. Rev.* **51,** 7–61 (1999).
3. Waxman, E. A. & Lynch, D. R. *N*-methyl-D-aspartate receptor subtypes: multiple roles in excitotoxicity and neurological disease. *Neuroscientist* **11,** 37–49 (2005).
4. Parsons, C. G., Danysh, W. & Quack, G. Glutamate in CNS disorders as a target for drug development: an update. *Drug News Perspect.* **11,** 523–569 (1998).
5. Auberson, Y. P. *et al.* 5-phosphonomethylquinoxalinediones as competitive NMDA receptor antagonists with a preference for the human 1A/2A, rather than 1A/2B receptor composition. *Bioorg. Med. Chem. Lett.* **12,** 1099–1102 (2002).
6. Waxman, S. G., Black, J. A., Stys, P. K. & Ransom, B. R. Ultrastructural concomitants of anoxic injury and early post-anoxic recovery in rat optic nerve. *Brain Res.* **574,** 105–119 (1992).
7. Lin, S. C. *et al.* Climbing fiber innervation of NG2-expressing glia in the mammalian cerebellum. *Neuron* **46,** 773–785 (2005).
8. Li, S., Mealing, G. A., Morley, P. & Stys, P. K. Novel injury mechanism in anoxia and trauma of spinal cord white matter: glutamate release via reverse Na^+-dependent glutamate transport. *J. Neurosci.* **19,** RC16 (1999).
9. Chiu, S. Y. & Kriegler, S. Neurotransmitter-mediated signalling between axons and glial cells. *Glia* **11,** 191–200 (1994).
10. Matute, C., Alberdi, E., Ibarretxe, G. & Sanchez-Gomez, M. V. Excitotoxicity in glial cells. *Eur. J. Pharmacol.* **447,** 239–246 (2002).
11. Ziak, D., Chvatal, A. & Sykova, E. Glutamate-, kainate- and NMDA-evoked membrane currents in identified glial cells in rat spinal cord slice. *Physiol. Res.* **47,** 365–375 (1998).
12. Das, S. *et al.* Increased NMDA current and spine density in mice lacking the NMDA receptor subunit NR3A. *Nature* **393,** 377–381 (1998).
13. McDonald, J. W., Althomsons, S. P., Hyrc, K. L., Choi, D. W. & Goldberg, M. P. Oligodendrocytes from forebrain are highly vulnerable to AMPA/kainate receptor-mediated excitotoxicity. *Nature Med.* **4,** 291–297 (1998).
14. Rosenberg, P. A. *et al.* Mature myelin basic protein-expressing oligodendrocytes are insensitive to kainate toxicity. *J. Neurosci. Res.* **71,** 237–245 (2003).
15. Lazzarini, R. A. *et al. Myelin Biology and Disorders* (Elsevier, Amsterdam, 2004).
16. Michailov, G. V. *et al.* Axonal neuregulin-1 regulates myelin sheath thickness. *Science* **304,** 700–703 (2004).
17. Quarles, R. H., Macklin, W. B. & Morell, P. in *Basic Neurochemistry* (eds Siegel, G. J., Albers, R. W., Brady, S. T. & Price, D. L.) 51–72 (Elsevier, San Diego, in the press).
18. Mrsulja, B. J., Zalewski, A. A. & Coping, G. Ultracytochemical localization of ouabain-sensitive K^+-dependent, p-nitrophenyl phosphatase in myelin. *Brain Res.* **343,** 154–158 (1985).
19. Kamasawa, N. *et al.* Connexin-47 and connexin-32 in gap junctions of oligodendrocyte somata, myelin sheaths, paranodal loops and

Schmidt-Lanterman incisures: implications for ionic homeostasis and potassium siphoning. *Neuroscience* **136,** 65–86 (2005).
20. Brand-Schieber, E. & Werner, P. AMPA/kainate receptors in mouse spinal cord: cell-specific display of receptor subunits by oligodendrocytes and astrocytes and at the nodes of Ranvier. *Glia* **42,** 12–24 (2003).
21. Li, S. & Stys, P. K. Mechanisms of ionotropic glutamate receptor-mediated excitotoxicity in isolated spinal cord white matter. *J. Neurosci.* **20,** 1190–1198 (2000).
22. Hinman, J. D., Duce, J. A., Siman, R. A., Hollander, W. & Abraham, C. R. Activation of calpain-1 in myelin and microglia in the white matter of the aged rhesus monkey. *J. Neurochem.* **89,** 430–441 (2004).
23. Mayer, M. L., Westbrook, G. L. & Guthrie, P. B. Voltage-dependent block by Mg^{2+} of NMDA responses in spinal cord neurones. *Nature* **309,** 261–263 (1984).
24. Aragon, C. & Lopez-Corcuera, B. Structure, function and regulation of glycine neurotransporters. *Eur. J. Pharmacol.* **479,** 249–262 (2003).
25. Danbolt, N. C. Glutamate uptake. *Prog. Neurobiol.* **65,** 1–105 (2001).
26. Stys, P. K. White matter injury mechanisms. *Curr. Mol. Med.* **4,** 113–130 (2004).
27. Spike, R. C., Watt, C., Zafra, F. & Todd, A. J. An ultrastructural study of the glycine transporter GLYT2 and its association with glycine in the superficial laminae of the rat spinal dorsal horn. *Neuroscience* **77,** 543–551 (1997).
28. Bear, M. F. & Malenka, R. C. Synaptic plasticity: LTP and LTD. *Curr. Opin. Neurobiol.* **4,** 389–399 (1994).
29. Lipton, S. A. & Rosenberg, P. A. Excitatory amino acids as a final common pathway for neurologic disorders. *N. Engl. J. Med.* **330,** 613–622 (1994).
30. Wallstrom, E. *et al.* Memantine abrogates neurological deficits, but not CNS inflammation, in Lewis rat experimental autoimmune encephalomyelitis. *J. Neurol. Sci.* **137,** 89–96 (1996).

Supplementary Information is linked to the online version of the paper at www.nature.com/nature.

Acknowledgements This work was supported by the NINDS, CIHR, Heart and Stroke Foundation of Ontario Center for Stroke Recovery, an HSFO Career Investigator Award, the Canadian Institute for Photonic Innovations, and the generosity of private donors to P.K.S. G.W.Z. is a Canada Research Chair and an AHFMR Senior Scholar. This work was additionally supported by the CIHR (G.W.Z., J.E.M.) and NINDS (B.D.T.). We thank Y. Auberson for the gift of NVP-AAM077; J. A. Wang and C. E. Morris for providing HEK293 cells for fluorescence-lifetime measurements; and M. Nikolaeva for assistance with fluo-4 Ca^{2+} imaging.

Author Information Reprints and permissions information is available at npg.nature.com/reprintsandpermissions. The authors declare no competing financial interests. Correspondence and requests for materials should be addressed to P.K.S. (pstys@ohri.ca).

Supplementary Figures

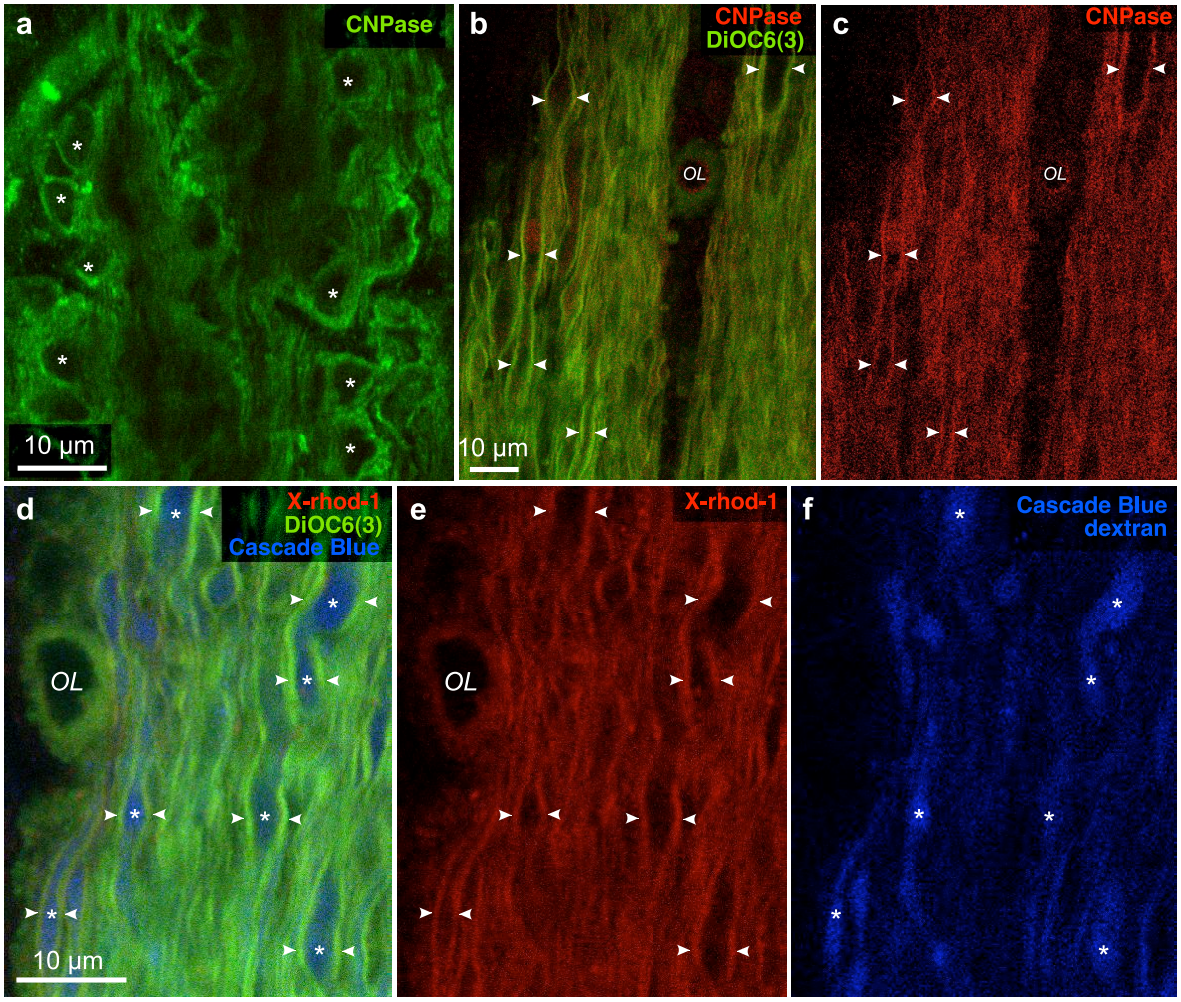

Supplementary Figure 1: Identification of oligodendrocytes and myelin. To ensure that ROIs selected as oligodenrocytes and myelin truly reflect the intended elements, some nerves were immunostained in-place on the microscope stage after completion of Ca^{2+} imaging experiments using standard markers. **a**, CNPase labels oligodendrocyte cell bodies and myelin[31]. Typical CNPase-positive rows of oligodendrocytes are seen (*), and correspond to the cell bodies stained with X-rhod-1 and DiOC6(3) as shown in panels b,d and e, and Fig.1 (*OL*). **b,c**, 2-photon micrograph of an optic nerve labeled with DiOC6(3)

then immunostained in-place using anti-CNPase antibody. Numerous bright DiOC6(3)-positive long parallel bands are seen that are also CNPase-positive, representing myelin sheaths. Thus, DiOC6(3) strongly stains myelin and is a convenient and reliable vital stain for this structure. **d,e,f**, 2-photon image of live optic nerve stained with DiOC6(3), the Ca^{2+} indicator X-rhod-1 and the dextran conjugate of cascade blue. The 10 kDa dextran conjugate restricts the blue dye to axon cylinders[32,33]. DiOC6(3) identifies myelin regions clearly: numerous parallel bands flanking cascade blue-loaded axon cylinders (*) represent myelin (arrowheads). X-rhod-1 loads into the DiOC6(3)-labeled linear myelin profiles (panel e) and cell bodies of oligodendrocytes (OL). Taken together, these data strongly support the conclusion that X-rhod-1 signals collected from DiOC6(3)-labeled linear profiles adjacent to axon cylinders originate from myelin. Scale bars 10 μm.

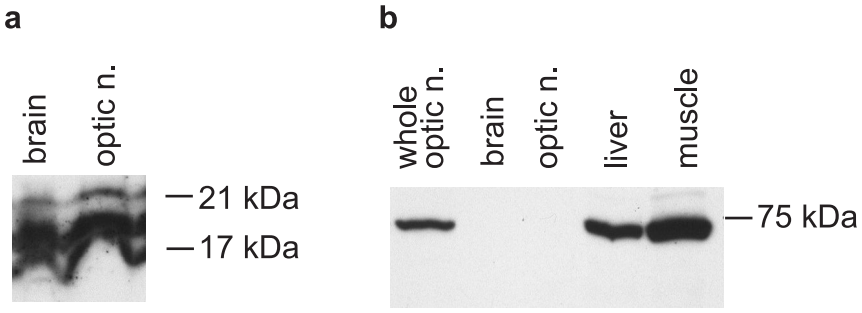

Supplementary Figure 2: Confirmation of the purity of myelin fractions. The myelin fraction from optic nerve was isolated on a sucrose gradient as described in Supplementary Methods #7. Immunoblots were performed on these fractions to ensure that appropriate markers are present and absent from the fractions. **a**, Very strong signal was seen for myelin basic protein, a major constituent of compact myelin, in fractions from both whole brain and optic nerves. **b**, endoplasmic reticulum integral membrane protein calnexin [34], a marker for cytoplasmic organelles, was present in whole (unfractionated) optic nerve, but was undetectable in isolated myelin from brain and optic nerves, confirming that the myelin fractions contained highly purified myelin with no detectable contamination from other cellular constituents.

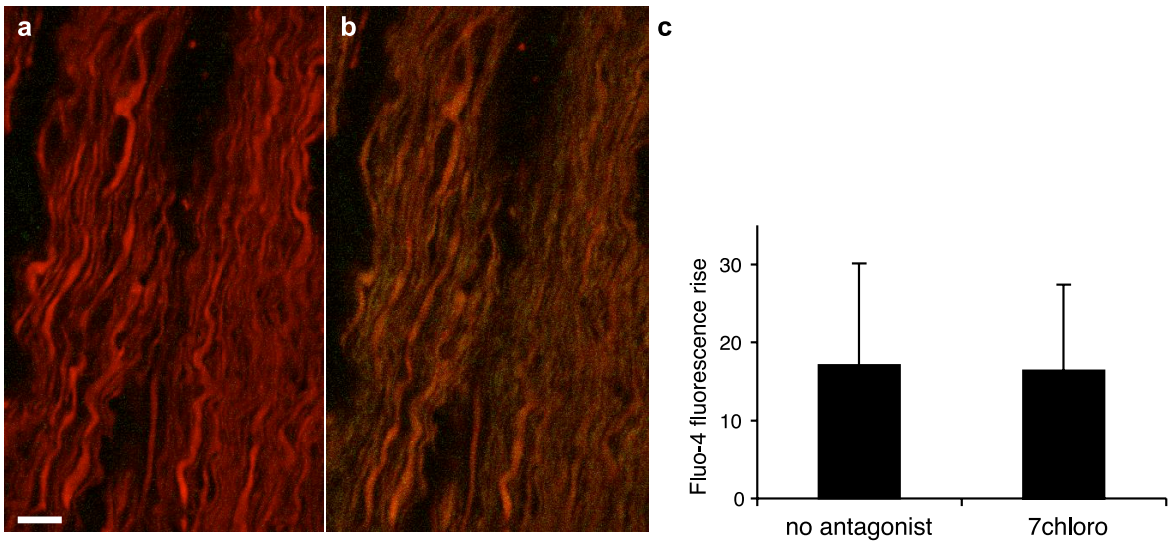

Supplementary Figure 3: Measurement of axoplasmic Ca^{2+} changes during chemical ischemia. Dextran-conjugated fluo-4 emission was measured from axon cylinders identified by the Ca^{2+}-insensitive indicator Alexa Fluor 594 dextran. **a**,example of control pre-ischemic optic nerve showing clearly outlined axon cylinders with virtually no green fluo-4 emission indicating very low resting Ca^{2+} levels in uninjured fibers. **b**, during chemical ischemia, Ca^{2+} levels in axons rose sharply as illustrated by greater green fluo-4 emission giving the axon cylinders a yellowish hue. **c**, bar graph summarizing the mean fluo-4 fluorescence intensity increase measured from axon cylinders after 30 min of chemical ischemia. Axons in aCSF+vehicle exhibited a 17±13 -fold increase in emission intensity (n=64 axons), and in the presence of the NMDA receptor antagonist 7-chlorokynurenic acid (200 μM), the ischemic axonal Ca^{2+} increase was not reduced (16±11-fold increase, n=100, p=0.69), indicating that, in contrast to oligodendrocyte cell bodies and myelin, NMDA receptors do not contribute significantly to Ca^{2+} loading of ischemic axons. Scale bar 10 μm.

Supplementary Methods

1. Ca^{2+} imaging of live optic nerves

Adult Long Evans rats (200-250 g) were deeply anesthetized and optic nerves dissected free as previously described[35]. Nerves were incubated in a solution of aCSF (containing in mM: NaCl 126, $NaHCO_3$ 26, KCl 3, NaH_2PO_4 1.25, $MgSO_4$ 2, dextrose 10, bubbled with 95%O_2/5%CO_2, pH 7.4) with Ca^{2+} omitted and with the addition of 1 mM EGTA to keep the cut ends of axons open. The Ca^{2+} indicator X-rhod-1 (http://probes.invitrogen.com/handbook/sections/1903.html) (nominal Kd for Ca^{2+} ≈700 nM, peak emission at 610 nm) was added to the solution as the acetoxymethyl ester (38 μM), along with DiOC6(3) (500 nM) to label myelin. Dextran-conjugated Ca^{2+}-insensitive Cascade Blue (180 μM) was transported down axons from the open cut ends, selectively labeling axon cylinders[33,36] (Fig.1, Supplementary Fig. 1) . Nerves were loaded in this fashion at room temperature for 2 hrs, then transferred to aCSF containing 2 mM Ca^{2+} at 35°C for 30 min to allow de-esterification of the acetoxymethyl ester and wash of excess dyes. Samples were then transferred to a perfusion chamber on the microscope stage and bathed with Ca^{2+}-replete aCSF at 36°C.

Two-photon excited fluorescence images were collected every 2 min using a custom modified Nikon D-Eclipse C1 laser scanning microscope. Samples were excited with ≈ 50 fs pulses at 925 nm (determined to be optimal by wavelength scanning at constant average laser power). Emitted fluorescence was collected using appropriate filters. Image data were imported into *ImageTrak* software (written by PKS; http://www.ohri.ca/stys/imagetrak) for

analysis. All quantitative fluorescence changes are reported after a standard 30 min ischemic exposure. In-place immunohistochemistry of live nerves was performed to ascertain the localization of X-rhod-1. Fluorescence lifetime measurements confirmed that fluorescence intensity of X-rhod-1 reported [Ca^{2+}] changes, and Mn^{2+} quench studies showed that emission originated from the cytosolic compartment of myelin.

Although DiOC6(3) and X-rhod-1 both partitioned strongly into myelin, experiments using X-rhod-1 labeling alone or in combination with DiOC6(3) yielded similar results indicating that there was no artifactual interaction between these two dyes that may have skewed the Ca^{2+} measurements provided by X-rhod-1. Because X-rhod-1 may have been operating near its saturation level at 30 min of ischemia (in which case minor effects of seemingly ineffective antagonists such as ifenprodil could have been obscured), ischemia was repeated in 1 mM bath Ca^{2+} to reduce the myelinic Ca^{2+} increase, ensuring that X-rhod-1 was not saturated and remained in a state where it could report additional increases or decreases in Ca^{2+}-dependent fluorescence. At 30 min, fluorescence increased to 14±6% (n=24) above baseline, well below the ≈50% increase observed in 2 mM Ca^{2+}, ensuring that in 1 mM Ca^{2+} the dye was operating below saturation. Addition of ifenprodil did not reduce the fluorescence increase (15±7% rise, n=25, p=0.25), therefore the lack of effect was real and not obscured by saturation of the indicator by potentially high myelinic [Ca^{2+}].

For Ca^{2+} measurements in axoplasm (as opposed to myelin), optic axons were loaded with Ca^{2+}-insensitive Alexa Fluor 594 dextran and the low affinity (Kd ≈ 4 μM) Ca^{2+} indicator fluo-4 dextran, and imaged in confocal mode as recently described [37].

2. Identification of myelin ROIs by in-place immunohistochemistry

The precise location of the various fluorescent indicators was confirmed on anatomical grounds and by immunohistochemistry of live nerves performed in-place after the completion of Ca^{2+} imaging experiments. Adult rat optic nerve axons are all fully myelinated[38]. In order to ensure that ROIs include only myelin we rely on the predictable geometry of adult myelinated axons. The ratio of axon (cylinder alone) diameter (a) to total myelinated fiber diameter (D) is fairly constant at about 0.7[38]. The myelin thickness on either side is therefore $m \approx 0.21a$. The a dimension is conveniently outlined by dextran loading of axons (e.g. cascade blue dextran signal in Fig. 1, Supplementary Fig. 1). Therefore by selecting ROIs that lie immediately adjacent to fluorescent dextran-loaded axon cylinders and extend outwards no further than ≈20% of the axon diameter a, we can be confident that the region will include mostly compact myelin. To further confirm that ROIs selected with the above method and directly labeled with DiOC6(3) represent myelin, optic nerves were immunostained in-place on the microscope stage after the completion of Ca^{2+} imaging experiments (Supplementary Fig. 1). At the end of some experiments optic nerves were maintained in position on the microscope stage and fixed with 4% paraformaldehyde in 0.1M phosphate buffer for 15 min and then washed 5 min with 0.1 M PBS buffer. Nerves were then incubated with primary antibodies that recognize oligodendrocytes and myelin (anti-CNPase[31]), 2% normal goat serum and Triton 3% in 0.1M PBS buffer then incubated with secondary antibody, and subsequently washed with aCSF. Controls consisted of primary antibodies omitted. Because of optical resolution limits, ROIs mainly represented larger (>1 μm) diameter axons and their myelin sheaths.

3. Confirmation of X-rhod-1 partitioning into the cytosolic subcompartment of myelin

X-rhod-1 is a cationic Ca^{2+} reporting dye selected based on the expectation that its lipophilicity would allow it to preferentially partition into the lipid rich myelin compartment, and its cationic nature would drive it into the cytosolic domain (the majore dense line) of myelin formed by the near-apposition of two layers of oligodendrocytic membrane. The following observations strongly favor the argument that de-esterified X-rhod-1 was reporting Ca^{2+} changes from this cytosolic domain, and not from the extracellular space of myelin wraps. Addition of 500 μM Mn^{2+} to a 10 μM X-rhod-1 (salt) solution in aCSF containing ≈1.5 mM free Ca^{2+} reduced fluorescence by ≈60%, confirming that Mn^{2+} ions can quench X-rhod-1 fluorescence. Optic nerves were loaded with X-rhod-1 and imaged as described. Perfusing resting nerves with solution containing 500 μM Mn^{2+} did not quench X-rhod-1 emission from myelin regions (14% intensity *increase* following 30 min of Mn^{2+} exposure). This suggests that if X-rhod-1 signal originated even partially from dye located in the extracellular space of myelin, entry of Mn^{2+} into this space should have quenched and reduced its emission. This result indicates that X-rhod-1 and Mn^{2+} remained in different compartments (the former intracellular, the divalent cation restricted to the extracellular domain). There still existed the possibility that Mn^{2+} was simply unable to permeate the tight interstices of the myelin spirals, even though large trivalent cations such as La^{3+} and even small proteins (microperoxidase, MW 2000) can enter under the myelin into the peri-axonal space[39,40]. In contrast to control optic nerves, X-rhod-1 signal from myelin regions in chemically ischemic nerves *decreased* by 30% (time-matched ischemic nerves displayed a slight 10-20% *increase* in X-rhod-1 fluorescence without

addition of Mn^{2+}, confirming that the observed reduction was an effect of Mn^{2+}, and not dye loss/photobleaching with longer imaging times) . Mn^{2+} has been shown to block and even permeate NMDA receptors [41,42]. Its ability to quench myelinic X-rhod-1 fluorescence in *ischemic*, but not *resting*, nerves can be explained either by its NMDA receptor blocking action (and we show here that these receptors play a major role in raising myelinic [Ca^{2+}]) and/or permeation through activated NMDA receptors then quenching fluorescence from the cytosolic domain of myelin. Importantly, this result proves that Mn^{2+} was able to diffuse into the tight myelin spirals, but was excluded from the cytosolic domain unless NMDA receptors were activated. We therefore infer that most of the X-rhod-1 fluorescence measured from myelin regions originated from this cytosolic domain.

4a. Fluorescence lifetime measurements of X-rhod-1 emission

Although X-rhod-1 was developed as a Ca^{2+} indicator, both the excitation and emission properties of fluorescent probes are also sensitive to properties of the medium in which they are embedded[43]. Fluorescence lifetime is a particularly sensitive measure of a fluorophore's local environment. Therefore, if lifetimes change little, one can infer that the environment remained stable and did not influence the emission of a dye *per se*. Using time-correlated single photon counting, we measured fluorescence lifetimes of X-rhod-1 loaded into HEK293 cells, to measure the characteristics of this dye in "prototypical" cytoplasm. In this compartment, decay times were bi-exponential with time constants of 0.47±0.05 and 2.39±0.22 ns (n=18), reflecting the Ca^{2+}-free and Ca^{2+}-bound forms of the dye. These decay times were somewhat different from pure aqueous solution containing 100 nM Ca^{2+} (≈ 0.23 and 3.4 ns), underscoring the effects of different environments (i.e.

simple aqueous Ca^{2+} buffer solution vs. complex cellular cytoplasm) on fluorescence decays. X-rhod-1 fluorescence lifetimes measured from myelin regions in control nerves (0.43±0.06 and 2.45±0.24 ns, n=31) were virtually identical to those measured in HEK293 cytoplasm, and exhibited little change after 30 min of chemical ischemia (0.40±0.07 ns, p=0.10, and 2.56±0.21 ns, p=0.09 vs. pre-ischemic myelin, n=17), despite a robust increase in emission intensity (Fig. 1). Taken together our fluorescence lifetime data indicate that X-rhod-1 in myelin reported from a compartment that was similar to cytoplasm. Moreover, chemical ischemia induced an increase in X-rhod-1 emission intensity without a significant change in fluorescence lifetime, strongly suggesting that this dye reported changes in $[Ca^{2+}]$, rather than being influenced by an unexplained environmental change in the cytoplasmic compartment of myelin.

4b. Time-correlated single photon counting (TCSPC)

Time resolved measurements were performed by TCSPC in a reversed start-stop mode. Light was directed to a Hamamatsu H7422P-40 photomultiplier whose output was passed through an Ortec Model 9327 amplifier discriminator. Green DiOC6(3) emission from myelin was split using a dichroic mirror and its signal integrated with a fast time-constant; this generated a gate signal for the TCSPC electronics, thus restricting photon counting to DiOC6(3)-emitting regions allowing us to determine X-rhod-1 lifetime from myelin in isolation. TCSPC was performed with an Ortec model 9308 time discriminator with stop trigger from the laser pulse provided by a fast diode with constant-fraction-discriminator (Becker & Hickl OCF-401). Cable lengths were adjusted to ensure that the trigger and fluorescence photon originated from the same laser pulse. Lifetime data were fit using

Fluofit [44]. The instrument response function was determined by second harmonic generation from crystalline potassium dihydrogen phosphate.

5. Electron microscopy

Freshly excised rat optic nerves were exposed to chemical ischemia @ 37°C for 1h, in aCSF containing either DMSO vehicle or 500 μM 7-chlorokynyrenic acid (in DMSO stock) to block NMDA receptors. Nerves were then immersed in cold fixative containing 1.6% glutaraldehyde in cacodylate buffer, and processed routinely for electron microscopy. Tissue was placed in capsules containing Spurr-resin and polymerized for 24 hours at 80°C. Blocks were trimmed and the tissue cut at 60 nm thickness onto copper grids, stained with uranyl acetate and lead citrate, and viewed using a Hitachi 7100 transmission electron microscope. Grids were examined by an experienced neuropathologist (JW) blinded to the treatment conditions. The number of myelin separations (arrowheads, Fig. 4a) per unit area was counted in 9 randomly selected regions (65 μm^2 each) from each treatment group, allowing a statistical and quantitative comparison of myelin pathology without and with NMDA receptor antagonist. The DMSO vehicle alone had no detectable effects on ischemic ultrastructural changes (results not shown).

6. Immunogold labeling

Tissue for immuno-gold labeling (Fig. 3e-h) was prepared from deeply anesthetized adult rats perfused with 2.5% glutaraldehyde, 4% paraformaldehyde, and 0.08 M Sorrenson's buffer. Optic nerves were infiltrated with 2.3 M sucrose and 30% polyvinylpyrrolidone, placed on specimen stubs, and frozen in liquid nitrogen. Ultrathin cryosections were cut on

glass knives in a Reichart Ultracut S (Leica Instruments) at –110 °C. The sections were placed on carbon- and Formvar-coated grids and immunostained as previously described[45]. Briefly, sections were stained by floating the grids sequentially on drops of the following solutions: 10% ovalbumin, 3% normal goat serum and PBS for 30 min; primary antibodies (anti-pan-NR1 monoclonal [Calbiochem # 454578], NR2 polyclonal [Affinity BioReagents # OPA-04020], NR3A&B monoclonal [Chemicon # MAB5388]), 1% ovalbumin and 0.3% normal goat serum (PBS-1) overnight at 4°C; PBS rinse (6x5 min); colloidal gold-labeled secondary antibodies and PBS-1 for 1 hr; and PBS rinse (6x5 min). The grids were then placed in 2.5% glutaraldehyde in PBS for 15 min and rinsed in PBS (4x5 min) and distilled water (4x2 min). The sections were then stained with neutral uranyl acetate and embedded in 2% methylcellulose containing 0.3% uranyl acetate. Grids were examined on a Philips CM-100 electron microscope.

7. Myelin fractionation

Myelin was isolated according to the procedure of Norton and Poduslo[46]. Briefly, optic nerves were homogenized in 0.32 M sucrose, the homogenates layered over 0.83 M sucrose and centrifuged at 75,000 g x 30 min, and the interphase myelin fraction collected. The fraction was further washed with water and centrifuged at 75,000 g x 10 min, hypotonic shocked twice at low-speed centrifugation 12,000 g x 10 min, then layering was repeated to obtain pure myelin. Purity of the extract was assessed by immunoblotting for standard markers (see Supplementary Fig. 2).

8. Immunoblots/immunoprecipitation

Myelin fractions were incubated on ice for 1 hour, centrifuged for 15min (4ºC) at 15000g and the supernatant collected for overnight dialysis against the binding solution (300 mM NaCl, 50mM Tris pH 7.5 and 0.1% Triton X-100). 250µg of total protein (50µl) was mixed with pan-NR1 monoclonal antibody (1:100 dilution; Calbiochem). The mixture was incubated overnight at 4ºC with rotation. 100 µl of precleared Protein G-Sepharose was used for the NR1 monoclonal. The mixture was incubated at room temperature for 1 hour and then the solution was washed two times with Buffer B (0.2% NP-40, 10 mM Tris pH 7.5, 0.15 M NaCl and 2mM EDTA) one time with Buffer C (as in B but 0.5 M NaCl), one time with Buffer D (10 mM Tris, pH 7.5). The complex was centrifuged and resuspended in 25 µl 3M urea/10 mM Tris pH 7.5 plus and additional 25 µl of 2X's sample buffer was added to each sample, boiled 5 minutes and loaded onto a 6% acrylamide SDS-PAGE gel. The samples were transferred to PVDF membrane and Western analysis was performed using a different NR1 polyclonal (1:500), NR2 polyclonal (1:1000) or NR3 monoclonal, and detected using ECL. Appropriate negative controls were performed by omitting the primary precipitating antibody or probing with secondary only (data not shown).

9. Reagents

Salts and pharmacological agents were from Sigma unless otherwise specified.

Antibodies (primaries and secondaries):

- CNPase: Chemicon
- Alexa Fluor 405, 594: Molecular Probes
- pan-NR1: polyclonal, Upstate (#07-362); Chemicon (#AB1516)
- NR2: polyclonal, Affinity BioReagents # OPA1-04020 (recognizes NR2A, 2B and 2C; based on sequence homology in the N-terminal region which was used to raise this antibody, we cannot rule out the possibility of cross-reactivity with NR2D).
- NR3: monoclonal recognizes NR3A and B (Chemicon # MAB5388); polyclonal recognizes NR3A (Upstate # 07-356)
- NF160: Sigma
- donkey anti-mouse, anti-rabbit Cy2, anti-mouse Texas Red, gold-conjugated secondaries: Jackson ImmunoResearch Labs

Supplementary Notes

1. Statistics

Means are shown with standard deviations. Statistical differences were computed using ANOVA with Dunnett's test for multiple comparisons with a common control group using Igor (Wavemetrics. Lake Oswego, OR). Levene's test was used to verify homogeneity of variance. Significance was accepted for $p < 0.01$. N's are myelin regions from individual axons.

2. Abbreviations

aCSF	artificial cerebrospinal fluid
AMPA	alpha-amino-3-hydroxy-5-methyl isoxazole propionic acid
CNPase	2', 3'-cyclic nucleotide 3'-phosphodiesterase
CNS	central nervous system
DAP5	D-2-amino-5-phosphonopentanoic acid
DiOC6(3)	3,3'-dihexyloxacarbocyanine iodide
DMSO	dimethyl sulfoxide
ECL	enhanced chemiluminescence
EDTA	ethylenediaminetetraacetic acid
EGTA	ethylene glycol bis(2-aminoethyl ether)-N,N,N'N'-tetraacetic acid
$F_{Ca.ol}$, $F_{Ca.my}$	Ca^{2+}-dependent X-rhod-1 fluorescence from oligodendrocytes, myelin
HIV	human immunodeficiency virus
PVDF	polyvinyl difluoride
NBQX	2,3-dihydroxy-6-nitro-7-sulphamoyl-benzo(F)quinoxaline
NMDA	N-methyl-D-aspartate
NVP-AAM077	[(R)-[(S)-1-(4-bromo-phenyl)-ethylamino]-(2,3-dioxo-1,2,3,4-tetrahydroquinoxalin-5-yl)-methyl]-phosphonic acid
ROI	region of interest
SDS-PAGE	sodium dodecyl sulfate-polyacrylamide gel electrophoresis

3. Author Contributions

IM: experimental concept and design, 2-photon Ca^{2+} imaging, fluorescence lifetime measurements, numerical data analysis, in-place immunohistochemistry and confocal microscopy, major role in writing of manuscript. QJ: myelin fractionation, immunoblots. EC: immunohistochemistry, confocal microscopy. AR, LZ: 2-photon microscopy, fluorescence lifetime measurements and associated numerical data analysis. JW,WW: ultrastructure of ischemic nerve. XY, BDT: immuno-electron microscopy. JEM, RR, GWZ: co-immunoprecipitation and immunoblots for NR subunits. PKS: experimental concept and design, coordination of experiments and data analysis, writing of manuscript. All authors were involved with analysis and interpretation of their respective data, and contributed to the writing of the paper.

4. References

31. Trapp, B. D., Bernier, L., Andrews, S. B. & Colman, D. R. Cellular and subcellular distribution of 2',3'-cyclic nucleotide 3'-phosphodiesterase and its mRNA in the rat central nervous system. *J. Neurochem.* **51**, 859-868 (1988).

32. Ouardouz, M. et al. Depolarization-induced Ca^{2+} release in ischemic spinal cord white matter involves L-type Ca^{2+} channel activation of ryanodine receptors. *Neuron* **40**, 53-63 (2003).

33. Verbny, Y., Zhang, C. L. & Chiu, S. Y. Coupling of calcium homeostasis to axonal sodium in axons of mouse optic nerve. *J. Neurophysiol.* **88**, 802-16. (2002).

34. Wada, I. et al. SSR alpha and associated calnexin are major calcium binding proteins of the endoplasmic reticulum membrane. *J. Biol. Chem.* **266**, 19599-19610 (1991).

35. Stys, P. K., Ransom, B. R. & Waxman, S. G. Compound action potential of nerve recorded by suction electrode: a theoretical and experimental analysis. *Brain Res.* **546**, 18-32 (1991).

36. Ren, Y., Ridsdale, A., Coderre, E. & Stys, P. K. Calcium imaging in live rat optic nerve myelinated axons in vitro using confocal laser microscopy. *J. Neurosci. Meth.* **102**, 165-176 (2000).

37. Nikolaeva, M. A., Mukherjee, B. & Stys, P. K. Na^+-dependent sources of intra-axonal Ca^{2+} release in rat optic nerve during *in vitro* chemical ischemia. *J. Neurosci.* **25**, 9960-9967 (2005).

38. Foster, R. E., Connors, B. W. & Waxman, S. G. Rat optic nerve: electrophysiological, pharmacological and anatomical studies during development. *Dev. Brain Res.* **3**, 371-386 (1982).

39. Feder, N. Microperoxidase. An ultrastructural tracer of low molecular weight. *J. Cell Biol.* **51**, 339-343 (1971).

40. Hirano, A. & Dembitzer, H. M. Further studies on the transverse bands. *J. Neurocytol.* **11**, 861-866 (1982).

41. Mayer, M. L. & Westbrook, G. L. Permeation and block of N-methyl-D-aspartic acid receptor channels by divalent cations in mouse cultured central neurones. *J. Physiol.* **394**, 501-527 (1987).

42. Simpson, P. B., Challiss, R. A. & Nahorski, S. R. Divalent cation entry in cultured rat cerebellar granule cells measured using Mn^{2+} quench of fura 2 fluorescence. *Eur. J. Neurosci.* **7**, 831-840 (1995).

43. Lakowicz, J. R. *Principles of Fluorescence Spectroscopy* (Plenum Publishing, 1999).

44. Enderlein, J. & Erdmann, R. Fast fitting of multi-exponential decay curves. *Optics Commun.* **134**, 371-378 (1997).

45. Trapp, B. D. et al. Polarization of myelinating Schwann cell surface membranes: role of microtubules and the trans-Golgi network. *J. Neurosci.* **15**, 1797-1807 (1995).

46. Norton, W. T. & Poduslo, S. E. Myelination in rat brain: method of myelin isolation. *J. Neurochem.* **21**, 749-757 (1973).